SNR-weighted Sinogram Smoothing with Improved Noise-resolution Properties for Low-dose X-ray Computed Tomography

T. Li[*a], J. Wang[a], J. Wen[a], X. Li[b], H. Lu[c], J. Hsieh[d], and Z. Liang[a]

[a] State University of New York at Stony Brook, NY 11794, USA
[b] Columbia University, USA
[c] The Fourth Medical University. Xi'An, China
[d] GE Medical System, USA

ABSTRACT

To treat the noise in low-dose x-ray CT projection data more accurately, analysis of the noise properties of the data and development of a corresponding efficient noise treatment method are two major problems to be addressed. In order to obtain an accurate and realistic model to describe the x-ray CT system, we acquired thousands of repeated measurements on different phantoms at several fixed scan angles by a GE high-speed multi-slice spiral CT scanner. The collected data were calibrated and log-transformed by the sophisticated system software, which converts the detected photon energy into sinogram data that satisfies the Radon transform. From the analysis of these experimental data, a nonlinear relation between mean and variance for each datum of the sinogram was obtained. In this paper, we integrated this nonlinear relation into a penalized likelihood statistical framework for a SNR (signal-to-noise ratio) adaptive smoothing of noise in the sinogram. After the proposed preprocessing, the sinograms were reconstructed with unapodized FBP (filtered backprojection) method. The resulted images were evaluated quantitatively, in terms of noise uniformity and noise-resolution tradeoff, with comparison to other noise smoothing methods such as Hanning filter and Butterworth filter at different cutoff frequencies. Significant improvement on noise and resolution tradeoff and noise property was demonstrated.

Keywords: High resolution reconstruction, circular harmonic decomposition, conjugate gradient, fan-beam, uniform attenuation, resolution variation.

1. INTRODUCTION

It is well known that the quality of computed tomography (CT) images would be severely degraded by the excessive quantum noise under extremely low x-ray dose circumstances. Statistical iterative reconstruction with accurate modeling of the noise, rather than a filtered back-projection (FBP) with low-pass filtering, is one way to deal with the problem. It requires an accurate/realistic statistical model of the whole system behavior including the x-ray source, the object, and the detector. In the previous work of Elbakri *et al*. [1], the detected photon numbers were considered to follow a Poisson distribution plus a background Gaussian noise with zero mean. A penalized Poisson likelihood was then maximized to reconstruct the object image. Recently, they refined the likelihood model as a compound Poisson distribution as proposed by Whiting *et al*. [2], which accounts for both the energy spectrum of x-ray beam and the characteristics of the energy-integrating sensors in the x-ray CT detector [3]. Statistical image reconstruction usually outperforms the FBP-plus-low-pass-filter method as noise increases, because of a more accurate noise model being incorporated. In practice, however, modeling the entire data-acquisition process exactly is challenging, due to the complexity of the whole CT system, such as the use of the bow-tie filter, the calibration for the source and detectors, and *etc*. Furthermore, a sophisticate model often leads to great difficulties in optimizing the complicated penalized-likelihood cost function [3].

Another strategy is to estimate a noise-free sinogram from the noisy data, and then to reconstruct the object image from the estimation by FBP, which offers the exact solution for the noise-free projection data. This approach is often more computationally efficient than the iterative reconstruction through the image space, and also renders a more uniform and isotropic image resolution [4, 5]. Recently, La Rivière *et al*. extended their nonparametric regression approach from emission tomography to x-ray CT to fit the 1D (one-dimensional) profile for each scan angle [6, 7].

[*] tfli@mil.sunysb.edu; phone 1 631 444-7999; fax 1 631 444-6450

Medical Imaging 2004: Image Processing, edited by J. Michael Fitzpatrick, Milan Sonka, Proceedings of SPIE Vol. 5370 (SPIE, Bellingham, WA, 2004)
1605-7422/04/$15 doi: 10.1117/12.535560

They modeled the detected photon numbers also by a shift Poisson approximation [1], but ignored the effect of polyenergetic spectrum of the x-ray beam and the detector integrating property.

Our intention in this paper is to model the *sinogram* data after system calibrations rather than the raw data of the photon numbers. In current clinical x-ray CT systems, the system calibration is a critical step for generating high quality images for diagnosis, which includes source/detector calibration, beam hardening correction, and logarithm transformation and *etc*. These transformations alter the statistics of the acquired data dramatically, and make an accurate modeling intractable analytically. By our previous work and others in the literature, the calibrated sinogram is believed to approach a Gaussian distribution, with nonlinear signal-dependent variance [8]. In order to obtain a more accurate model to describe the x-ray CT system, we have acquired thousands of repeated measurements on different phantoms under various conditions using a GE high-speed multi-slice spiral CT scanner, and established a quite accurate empirical formula to describe the mean and variance relation in the Gaussian model. Based on this formula, the signal-to-noise ratio (SNR) could be estimated for every detector bin or pixel in the sinogram image. Therefore, a SNR-weighted nonlinear smoothing method can be developed by maximization of a penalized likelihood cost function.

In this paper, we also analyzed the reconstructed images after the proposed sinogram smoothing, and calculated the regional SNR and resolution of the local impulse response (LIR) under different smoothing levels. The noise uniformity and the resolution-noise tradeoff of the reconstructed images were then compared with the conventional Hanning and Butterworth filtering methods at different cutoff frequencies, where superior performance of the proposed method was observed. Furthermore, by experimental phantom data scanned with 120 kVp and 10 mA protocols, this approach demonstrated a remarkable improvement of the image quality, as compared to the conventional low-pass Hanning and Butterworth filters.

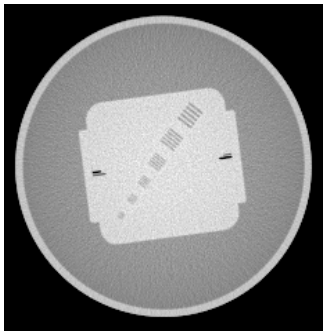
(a)

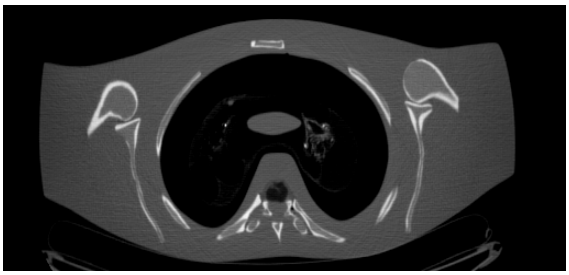
(b)

Figure 1. Physical phantoms used in the repeated fix-angle projections for noise property analysis. Picture (a) is a quality assurance (QA) phantom, and (b) is a thorax phantom.

2. METHODS

2.1 Noise model

In transmission tomography, the underlying equation governs the imaging is the Radon transform. For x-rays, if I_0 is the intensity of the source, $A(r)$ is the linear attenuation coefficient of the object at point r, L is the ray along which the radiation propagates, and I is the intensity of the radiation past through the object, then

$$\int_L A(r)dr = \ln \frac{I_0}{I} = g \qquad (1)$$

where a mono-energetic x-ray intensity is assumed. If we assume that I is a Poisson distributed random variable (r.v.) with mean value $\bar{I}$, and I_0 is some constant, then after log-transform, the mean and variance for sinogram g can be estimated via Taylor expansion as follows

$$g = \ln(I_0) - \ln(\bar{I}) + \ln(\bar{I}/I) \approx \ln(I_0) - \ln(\bar{I}) - \frac{I - \bar{I}}{\bar{I}}, \qquad (2)$$

and hence

$$\bar{g} = E(g) = \ln(I_0/\bar{I}), \qquad (3)$$

$$\sigma_g^2 = E(g^2) - E^2(g) = \frac{1}{\bar{I}}. \quad (4)$$

By equations (3) and (4), it is easy to see that

$$\sigma_g^2 \propto \frac{1}{I_0}\exp(\bar{g}) \quad (5)$$

Since it is generally believed that a Poisson r.v. after log-transform can be approximated by a Gaussian distribution [9], and also by the motivation of equation (5), we intend to find an accurate relation between the parameters of mean and variance in the Gaussian model for sinogram *g* scanned by a real CT system.

To analyze the probability distribution, we repeatedly acquired projection measurements of two physical phantoms at several fixed angles with a GE multi-slice spiral CT scanner. To see whether the distribution depends on the phantom being scanned or the imaging system, we chose two very different phantoms and scanned them with different machine settings. The first dataset was acquired for a nearly symmetric quality assurance (QA) cylinder phantom (see Figure 1(a)), and its repeatedly scannes were performed 900 times at 0 degree with 120 kVp, 20 mA protocol. The second and third datasets were acquired for a very asymmetrical thorax phantom, which was repeatedly scanned by 984 times at 0 degree and 90 degree, respectively, with 120 kVp, 50 mA protocol (see Figure 1(b)). The acquired three datasets were calibrated and log-transformed by the sophisticated system software, which converts the detected photon numbers into sinogram satisfying the Radon transform.

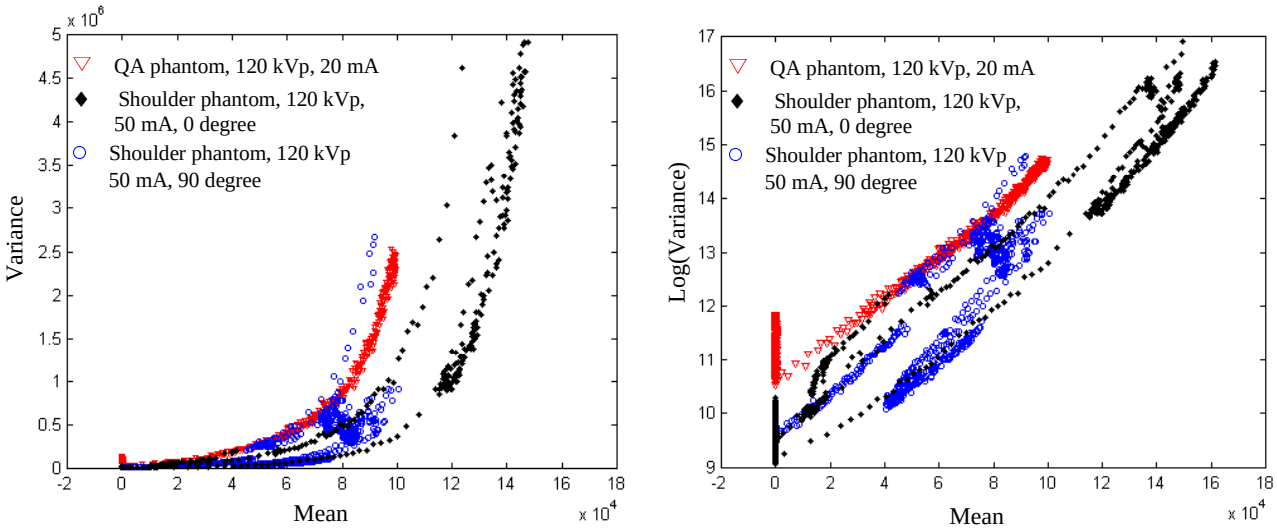

Figure 2. Left is the mean~variance curves for the three datasets: QA phantom scanned at 0 degree, 120 kVp and 20 mA; thorax phantom scanned at 0 degree, 120 kVp and 50 mA; thorax phantom scanned at 90 degree, 120 kVp and 50 mA. Each point in the plots represents the (μ_i, σ_i^2) value at detector bin *i*, which was estimated by the mean and variance of the large samples. Right is the plot of log(variance) ~ mean for the same datasets. Note that their slopes are nearly same, although the data are acquired from different objects at different machine settings.

For each dataset, we calculated the sample mean and sample variance as the unbiased estimation of the parameters in the Gaussian probability distribution function (PDF) $N(\mu_i,\sigma_i^2)$ and plotted them in Figure 2 (left), where *i* denotes different detector channel (or bin). Obviously a nonlinear dependency between μ_i and σ_i^2 is found in these datasets as shown in each mean-variance plot. In Figure 2 (right), the log(variance) versus the mean were re-plotted for the same data, where we found that the curves become straight lines and all have nearly same slopes – showing the same nonlinear dependency, although the scanned objects and machine settings are quite different among these data. Based on the observations of Figure 2, we proposed a model for the data mean and variance relation as follows

$$\sigma_i^2(\mu_i) = f_i \exp(\mu_i / T) \quad (6)$$

where T and f_i are object-independent coefficients. For the CT scanner used in this study, $T \approx 22000$, no matter what phantom or protocol is used, and f_i is shown in Figure 3. Equation (6) can be explained as follows: the calibrated sinogram for each channel follows a statistically independent Gaussian distribution. The variance of the data in any measurement is exponentially proportional to its expected mean value. The coefficient f_i reflects a non-uniform response or noise property across the detector bins. It would be affected by different system settings, which cause different fluctuation, and by background noise in the detector channels, (*e.g.*, f_i at 20 mA is about 4.5 times larger than that at 50 mA for each detector channel).

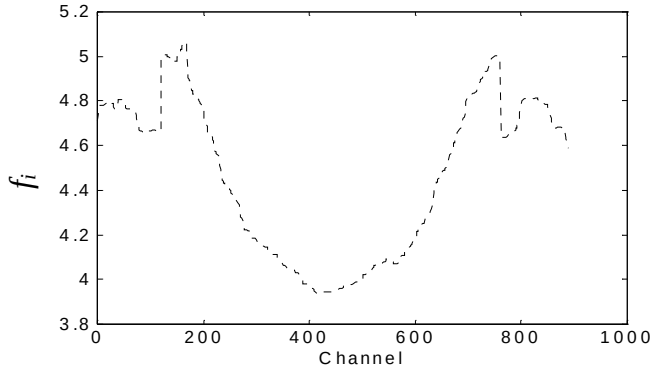

Figure 3. Coefficient f_i of the proposed formula for the mean-variance relation. Note that f_i varies with the detector channel i.

In order to validate the model above, we compared the experimental sample variance with the variance predicted by equation (6). Good consistency was observed for all three datasets. Figure 4 is an example for the comparison using data of thorax phantom scanned at 90 degree.

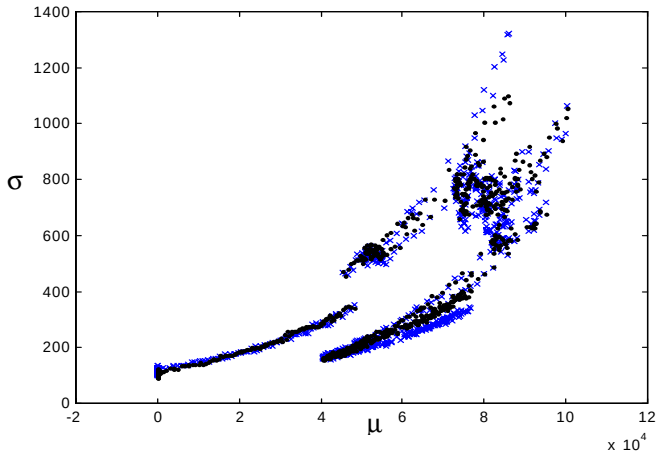

Figure 4: Comparison of sample variance and predicted one. The cross (x) is experimental data, the dot (.) is predicted data.

2.2 SNR-weighted penalized likelihood smoothing

With the Gaussian noise model and the mean-variance relationship, the Bayesian approach can be used to estimate a noise-free sinogram, which is based on the maximum *a posteriori* (MAP) criterion, or called penalized likelihood method. Denote by $P(\mu)$ the prior distribution for an unknown image $\mu = \{\mu_1, \mu_2, \cdots, \mu_N\}'$ (N is the total number of pixels in the sinogram image and notation $'$ denotes the transpose operation). Let X be the observed sinogram image $X = \{x_1, x_2, \cdots x_N\}'$, the MAP estimator is given by

$$\hat{\mu} = \arg\max_{\mu \geq 0} \{P(\mu|X)\} = \arg\max_{\mu \geq 0} \{P(X|\mu)P(\mu)\} \tag{7}$$

where the Bayesian formula has been used

$$P(\mu|X) = \frac{P(X|\mu)P(\mu)}{P(X)} \propto P(X|\mu)P(\mu) \cdot \tag{8}$$

It can be assumed that the observation at each pixel is independent from other observations [10], so that the conditional probability of observed image *X*, given the mean image μ, can be simply expressed as

$$P(X|\mu) = \prod_{i=1}^{N} p(x_i|\mu_i) = \prod_i \frac{1}{\sqrt{2\pi\sigma_i^2}} \exp\left(- \frac{(x_i - \mu_i)^2}{2\sigma_i^2} \right). \tag{9}$$

A general model for the prior distribution $P(\mu)$ is a Markov random field (MRF), which is characterized by the Gibbs distribution of

$$P(\mu) = \frac{1}{Z} \exp\left(- \frac{\alpha}{2} \mu' H \mu \right) \tag{10}$$

and is usually incorporated in the MAP estimation method [11,12]; where *Z* is a constant. In this paper, the core function of matrix *H* is designed slightly different from others [12]

$$\begin{bmatrix} 0 & -0.25 & 0 \\ -1 & 2.5 & -1 \\ 0 & -0.25 & 0 \end{bmatrix}, \tag{11}$$

and α is a weighting parameter that usually controls the smoothness of the result image. Since the variance is strongly dependent on the mean value and varies across the whole sinogram, it is preferable to adjust the smoothing-control parameter α according to the SNR at each location in the sinogram space. In this paper, we set the parameter proportional to the variance and, therefore, dependent on the detector reading according to variance-mean relation (6)

$$\alpha_i = \lambda \sigma_i^2 = \lambda f_i \exp(\hat{\mu}_i / T) \tag{12}$$

By taking the logarithm transform, the MAP estimation becomes a penalized weighted least-square (WLS) problem [13]:

$$\Phi(\mu) = \frac{1}{2}(X - \mu)' \Sigma^{-1} (X - \mu) + \frac{1}{2} \ln(2\pi\Sigma) + \frac{\alpha}{2} \mu' H \mu$$

$$\hat{\mu} = \arg\min_{\mu \geq 0} \Phi(\mu) \tag{13}$$

where $\Phi(\mu)$ denotes the cost function. The variance-covariance matrix Σ is diagonal with the *i*-th entry σ_i^2. To minimize equation (13), we take the partial derivatives with respect to μ_i and obtain the following non-linear equation set

$$\frac{(x_i - \mu_i)}{f} e^{-\mu_i / T} + \frac{(x_i - \mu_i)^2}{2fT} e^{-\mu_i / T} - \frac{T}{2} - \alpha [2.5\mu_i + \sum_{r \in N_i} w_r \mu_r] = 0, \quad i = 1,2,..., N \tag{14}$$

where *i* is the index of image pixel, *N* was defined before as the total number of pixels, and w_r is determined by equation (11). The summation in the last term comes from the neighborhood of pixel *i*. Rearrange equation (14), we can get the following iterated condition mode (ICM) iterative formula for the solution:

$$(\mu_i^{(n)} - (x_i + T))^2 - T^2 = [1 + 2\lambda(\sigma_i^2)^{(n-1)} T(2.5\mu_i^{(n)} + \sum_{r \in} w_r \mu_r^{(n-1)})](\sigma_i^2)^{(n-1)} . \tag{15}$$

Implementation of the ICM algorithm is straightforward, and the computation is efficient, as seen below:

(1) Initialize the mean image μ with the observed image X. (Since the expected value is close to the initial one, the local minimum is the convergent point that we are looking for and the convergence speed is fast.).

(2) Update the mean image μ pixel-by-pixel based on equation (9) and the variance σ_i^2 by equation (1).

(3) Repeat step 2 until it converges to point according to certain criteria. Usually 10 iterations are sufficient.

3 SIMULATION RESULTS

To evaluate the performance of the proposed approach, we first simulated a projection image with mathematical phantom shown in Figure 5 (left), then added it with signal-dependent Gaussian noise according to equation (6). The noisy sinogram data was then smoothed by our proposed method and reconstructed with FBP. Furthermore, for comparison purpose, the same noisy data was also reconstructed with Hanning filter and Butterworth filter with different cutoff frequency settings. These reconstructed images were analyzed and compared for the "noise uniformity" and resolution-noise tradeoff.

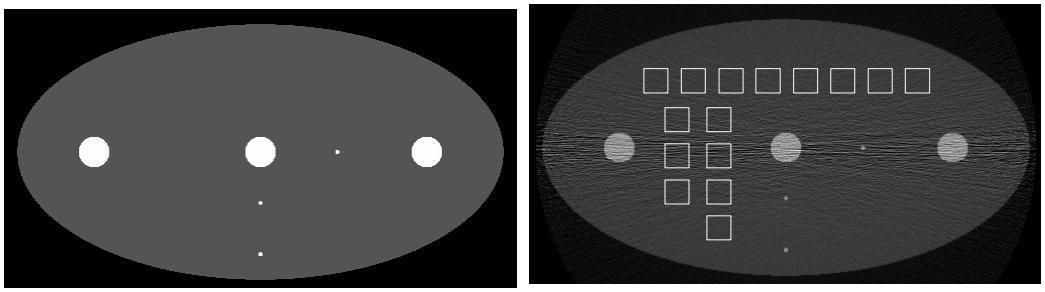

Figure 5. On the left is the phantom for simulation study, the three points A, B and C (one is on horizontal line with the three disks and two are in vertical line with one disk) are used to measure the local impulse response (or point spread function). Right one is a FBP reconstructed image from simulated noisy data without filtering. The squares in the right image indicate the locations for calculating the regional standard deviation and regional mean, each square contains 20x20 pixels.

3.1 Noise uniformity

As illustrated in Figure 5 (right), for the image reconstructed with each method, 15 representative regions were selected in uniform area to calculate the SNR, which we defined as the ratio of the local mean to the local standard deviation (SNR=mean/std). If the SNR does not vary much among all regions, the image has a uniform-noise property. In Figure 6, we plotted the SNRs calculated for each region with each method, where it is found that the proposed SNR-weighted approach can achieve more uniform noise across all selected regions, while the conventional Hanning filter or Butterworth filter resulted in much larger differences of SNRs in some regions.

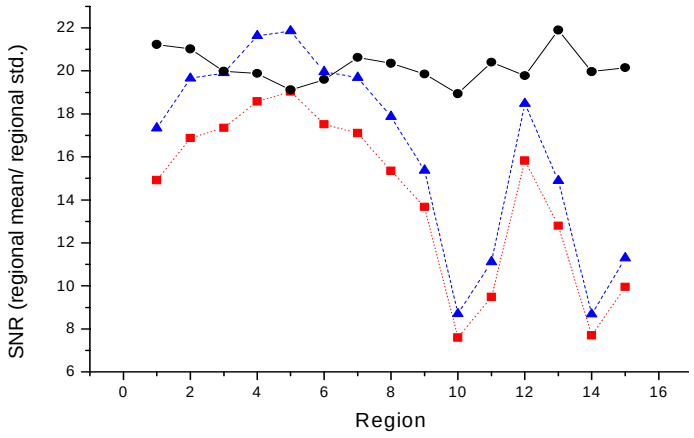

Figure 6. Regional SNRs calculated for different approaches. The circle with solid line is for the proposed approach (λ=5x10^{-8}), the upper-triangle with dash line is for Butterworth filter (order 3, cutoff at 25% Nyquist frequency), and the square with dot line is for Hanning filter (cutoff at 60% Nyquist frequency).

3.2 Resolution-noise tradeoff

Another important aspect for imaging system is the resolution-noise tradeoff. In computed tomography, reduction of the image noise usually leads to sacrifice of the spatial resolution. In order to quantify how the resolution changes with the smoothing level, we measured the full-width-at-half-maximum (FWHM, denoted by $W_{0.5}$), and the full-width at 1/e of the maximum (denoted by $W_{1/e}$), of the point spread function (PSF) in the reconstructed images, and the resolution is characterized by the "edge sharpness", *i.e.*, $W_{0.5} - W_{1/e}$, as illustrated in Figure 7.

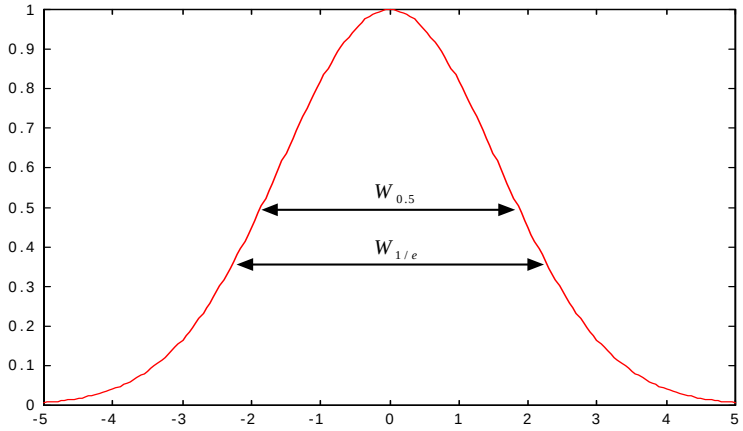

Figure 7. The resolution is measured by the sharpness of the point spread function, which is calculated by the difference of two widths $W_{0.5}$ and $W_{1/e}$. This definition can overcome the problem when the "point source" has a finite size.

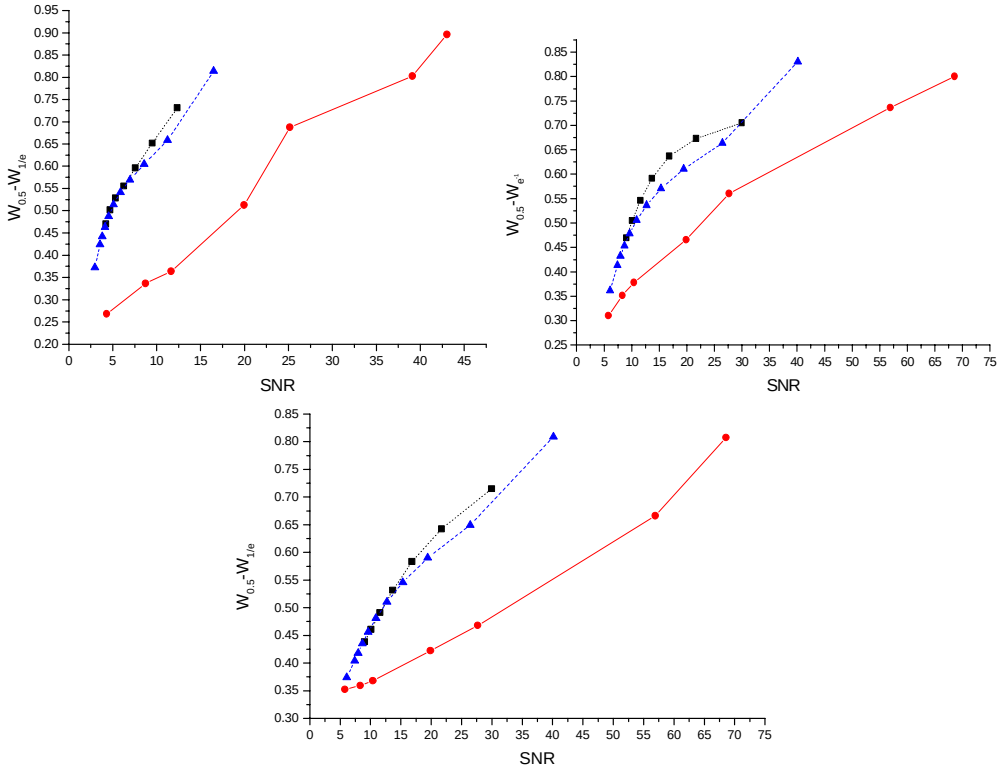

Figure 8. Plots of ($W_{0.5}$-$W_{1/e}$) versus SNR for demonstration of the resolution-noise trade-off for different approaches, measured at points A (up left), B (up right), and C (bottom). It can be found that, at the same spatial resolution (or width of $W_{0.5}$-$W_{1/e}$), the proposed approach gives much larger SNR.

With the proposed approach, the smoothness is controlled by adjusting parameter λ; for Hanning filter or Butterworth filter, it is controlled by the cutoff frequency f_c. For all methods, when the parameter setting increases the image SNR, (in another word, reduces the image noise), the spatial resolution gets worse, therefore, $W_{0.5}-W_{1/e}$ increases. In Figure 8, for each method, we plotted the width of $W_{0.5}-W_{1/e}$ versus the SNR corresponding to the three point sources A, B, and C illustrated in Figure 5, where the width is averaged over the horizontal and vertical profile of the PSFs. It can be found that, at the same spatial resolution (or width of $W_{0.5}$-$W_{1/e}$), the proposed approach will give much larger SNRs compared with Hanning or Butterworth filtering methods.

4 EXPERIMENTAL RESULTS

We further applied the SNR-weighted sinogram smoothing approach to experimental data, which was acquired by complete scan of a physical shoulder phantom at 120 kVp and 10 mA, using the GE high speed multi-slice CT scanner with fan-beam curved detector array. The distance from the center of rotation (COR) to the curved detector is 408.075 mm. The detector array is on an arc concentric to the x-ray source with a distance between the x-ray source and the COR of 541.00 mm. The detector cell spacing is 1.0239 mm. The number of channels per view was 888 with a total of 984 views evenly spanned on a circular orbit of 360^0. The detected photon counts were calibrated and logarithm transformed by the CT system. The outputs are the sinogram data satisfying the Radon transform.

The FBP reconstructed image without any noise treatment resulted in severe streak artifacts (see Figure 9 upper-left). With our proposed smoothing approach before FBP reconstruction, these artifacts are almost eliminated, and the image quality is improved dramatically (Figure 9 upper-right). For comparisons, reconstructions with low-pass Hanning and Butterworth filters are also shown in Figure 9 (bottom), where the cutoff frequencies were adjusted to achieve similar SNRs. From these pictures, we found the sinogram smoothing approach preserved much better spatial resolution over the simple low-pass filtering strategy.

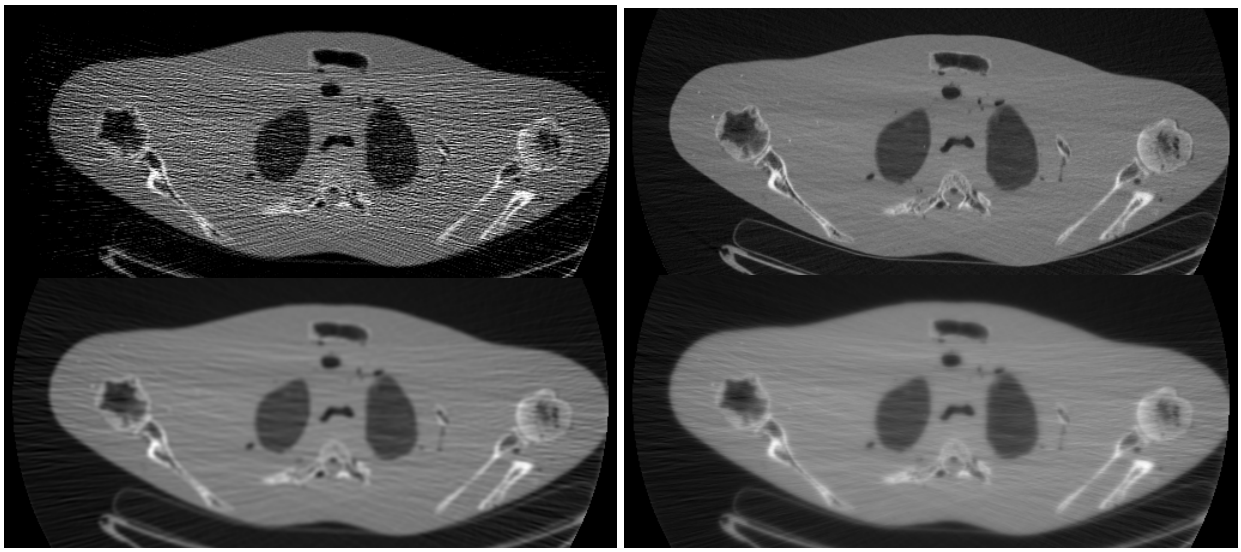

Figure 9: FBP reconstructed images for should phantom data scanned at 120 kVp, 10 mA. Upper-left is the reconstruction result from the original noisy data without noise treatment; upper-right is the reconstruction result with sinogram smoothing by the proposed method; bottom-left is the reconstruction with Hanning filter and cutoff at f_c=40% Nyquist frequency; bottom-right is the reconstruction with Butterworth filter of order 3 and cutoff at f_c=30% Nyquist. The parameters were set to achieve similar SNRs.

5 CONCLUSIONS

In this work, we first presented a novel statistic model for the x-ray CT data after system calibration and log-transform. With this empirical model, one can predict the variance, hence the noise property, of the sinogram very accurately.

Based on this model and *MAP* criterion, we then developed a nonlinear smoothing algorithm to perform the noise reduction for the sinogram, where the smoothness controlling parameter α is made inverse-proportional to the SNR. Reconstruction after this pre-processing of the sinogram showed superior performances in both simulation and experimental studies. First the noise uniformity is achieved, although the strong dependency of the variance upon the signal is present in the sinogram; secondly, the resolution-noise trade-off is greatly improved as well. Up to now, various forms of filtering techniques have been developed to smooth spatially the projection data and/or the reconstructed CT images, such as the adaptive trimmed mean filter, the non-linear anisotropic diffusion filter, and *etc* [14, 15]. Although they succeed in some degrees for noise reduction prior or post to image reconstruction, their assumed noise model is not justified in their applications and further development is then limited. The gain achieved by our method is expected because (i) the data is accurately modelled; (ii) the method explicitly employs the signal-dependent variance property and smoothes the sinogram data adaptively. The implementation of the proposed approach is very efficient. It should be noted that the ICM algorithm, adapted in this paper for the non-linear equation set, avoids directly solving for equation (9), which has exponential terms and is unstable. The variance is estimated in each iteration and substituted for the exponential terms according to equation (6), which makes the algorithm more robust and faster. The computing time for processing a sinogram of 888*x*984 pixel-array size is about 10 seconds on a PC Pentium II platform of 550Hz CPU.

Acknowledgement

This work was supported in part by the NIH National Heart, Lung and Blood Institute under Grant No. HL54166 and the NIH National Cancer Institute under Grant No. CA82402.

References

[1] I. A. Elbakri and J. A. Fessler, "Statistical image reconstruction for polyenergetic X-ray computed tomography", *IEEE Trans. Med. Imaging*, **21**: 89-99, 2002.
[2] B. R. Whiting. "Signal statistics in x-ray computed tomography", *SPIE Medical Imaging*, **4682**: 53-60, 2002.
[3] I. A. Elbakri and J. A. Fessler,, "Efficient and accurate likelihood for iterative image reconstruction in X-ray computed tomography", *SPIE Medical Imaging*, **5032**: 1839-1850, 2003.
[4] J. A. Fessler, "Tomographic reconstruction using information-weighted spline smoothing", in *Information Processing in Medical Imaging*, H. H. Barrett and A. F. Gmitro, Eds. Berlin, Germany: Springer-Verlag, 1993, pp. 290–300.
[5] Z. Liang, "Detector response restoration in image reconstruction of high resolution positron emission tomography", *IEEE Trans. Med. Imaging*, **13**: 314-321, 1994.
[6] P. La Rivière and X. Pan, "Nonparametric regression sinogram smoothing using a roughness-penalized Poisson likelihood objective function", *IEEE Trans. Med. Imaging*, **19**: 773-786, 2000.
[7] P. La Rivière, "Reduction of noise-induced streak artifacts in x-ray CT through penalized-likelihood sinogram smoothing", *Conf Record IEEE NSS-MIC*, 2003.
[8] H. Lu, X. Li, I. T. Hsiao, and Z. Liang, "Analytical treatment of noise for low-dose CT projection data by penalized weighted least-square smoothing in the K-L domain", *SPIE Medical Imaging*, **4682**: 146-152, 2002.
[9] A. Papoulis, *Probability, random variables, and stochastic processes*. McGraw-Hill, New York, 1965.
[10] T. Lei and W. Sewchand, "Statistical approach to x-ray CT imaging and its applications in image analysis - part I: Statistical analysis of x-ray CT imaging", *IEEE Trans. Med. Imaging*, **11**: 53-61, 1992.
[11] S. Geman and D. Geman, "Stochastic relaxation, Gibbs distributions and the Bayesian restoration of images", *IEEE Trans. Pattern Analysis and Machine Intelligence*, **6**: 721-741, 1984.
[12] D. Lalush and B M W Tsui, "A generalized Gibbs prior for maximum a posteriori reconstruction in SPECT", *Physics in Medicine and Biology*, **38**: 729-741, 1993.
[13] J. A. Fessler, "Penalized weighted least-squares image reconstruction for positron emission tomography", *IEEE Trans. Med. Imaging*, **13**: 290-300, 1994.
[14] J. Hsieh, "Adaptive streak artifact reduction in computed tomography resulting from excessive x-ray photon noise", *Medical Physics*, **25**: 2139-2147, 1998.
[15] K. Demirkaya, "Reduction of noise and image artifacts in computed tomography by nonlinear filtration of the projection images", *SPIE Medical Imagin*g, **4322**: 917-923, 2001.